RESEARCH ARTICLE

Comparative study on boundary lubrication of Ti$_3$C$_2$T$_x$ MXene and graphene oxide in water

Wei SUN[1], Qingrui SONG[1], Kun LIU[1], Qing ZHANG[2], Zhensheng TAO[2], Jiaxin YE[1,*]

[1] *Institute of Tribology, School of Mechanical Engineering, Hefei University of Technology, Hefei 230009, China*

[2] *Institutes of Physical Science and Information Technology, Anhui University, Hefei 230601, China*

© The author(s) 2022.

Abstract: The emerging use of two-dimensional (2D) nanomaterials as boundary lubricants in water offers numerous benefits over oil-based lubricants; whereas the friction reduction varies significantly with nanomaterial type, size, loading, morphology, etc. Graphene oxide (GO) and Ti$_3$C$_2$T$_x$ MXene, a relatively new 2D material, are investigated as boundary lubricants in water in this study. The contact pair mainly includes Si$_3$N$_4$ balls and Si wafer. The results found (1) monodispersed GO offers better lubricity than monodispersed MXene under identical concentration and testing conditions; and (2) the mixed dispersion of GO and MXene (0.1 mg/ml: 0.1 mg/ml) produced the lowest friction coefficient of ~ 0.021, a value 4× and 10× lower than that produced by comparable mono-dispersions of GO or MXene, respectively. Wear track analysis, focused ion beam microscopy, *in-situ* contact observation, and atomic force microscopy (AFM) characterization suggest (1) GO nanoflakes have higher adhesion than MXene and are more easily adsorbed on the tribopairs' surfaces, and (2) GO/MXene tribofilm has a layered nanostructure constituting GO, MXene, amorphous carbon, and TiO$_2$. We further hypothesized that the high lubricity of GO/MXene results from the synergy of GO's high adhesiveness, MXene's load support ability, and the low shear strength of both constituents. The present study highlights the key role of tribofilm stability in water-based boundary lubrication using state-of-the-art 2D nanomaterials.

Keywords: Mxene; graphene oxide; water-based lubricant additives; boundary lubrication; adsorption film

1 Introduction

Tribological behavior (i.e., friction and wear) is probably the least understood subject in surface engineering yet often plays a critical role in determining mechanical assemblies' performance, longevity, and reliability. In industrial applications, fluid lubrication is often introduced to effectively reduce friction and wear of mechanical parts [1]. But the excessive use of oil lubricants poses a threat to the environment [2]. Water-based lubricants with two-dimensional (2D) nano-additives such as graphene or phosphorene are environment-friendly substitutes for oil lubricants due to their high lubricity and excellent mechanical/thermal properties [3, 4]. However, many 2D nano-additives are hydrophobic in nature and difficult to incorporate/distribute homogeneously when applied in aqueous conditions [5–7].

This disadvantage can potentially be overcome by introducing surface terminations during the synthesis of these 2D nano-additives [8]. A great example is graphene oxide (GO). To synthesize GO, the graphitic powder is oxidized to generate GO containing hydroxyl, epoxide, carbonyl, and carboxyl groups [9]. Subsequently, GO is exfoliated by sonication to mono-, bi-, or few-layer nanosheets. Due to its abundant surface functional groups, GO exhibits excellent dispersibility in water [10] and show excellent performance as lubricant additives in water even without any further pre-treatment ($\mu \approx 0.05$–0.1) [7, 11, 12]. The speculated

---

* Corresponding author: Jiaxin YE, E-mail: yejx@hfut.edu.cn

lubrication mechanism of GO mainly comprises the formation of a GO-adsorption film that prevents friction pairs from direct contact and leads to the alleviation of wear [13, 14].

Similar to GO synthesis, MXenes (early transition metal carbides/carbonitrides/nitrides), a relatively new class of 2D nanomaterials, are generally fabricated by exfoliating the layered MAX precursors in hydrofluoric acid or hydrochloric acid containing dissolved fluoride salts [15–17]. For example, $Ti_3C_2T_x$ nanosheets, the most studied member of the MXenes, can be synthesized by etching the Al layers in Ti_3AlC_2 MAX precursor and replacing them with hydroxyl-, oxygen-, or fluorine-terminated groups [18, 19]. The produced $Ti_3C_2T_x$ nanosheets are hydrophilic and can be well-dispersed in water.

In the field of tribology, the low shear strength of 2D MXene has been confirmed by both experimental [20] and theoretical studies [21]. The tunable mechanical properties [22] and low shear strength of $Ti_3C_2T_x$ nanosheets render them promising candidates for application in triboelectric nanogenerators [23], lubricant additives [24, 25], reinforcement phases in nanocomposites [26, 27], and matrix of solid lubricants [28–34]. Interestingly, literature reports on the effectiveness of $Ti_3C_2T_x$ MXene as a water-based lubricant additive are inconsistent. Marian et al. [35] firstly revealed that the tribological performance of $Ti_3C_2T_x$ MXene tends to worsen in high humid environments. Nguyen and Chung [36] reported a friction coefficient of ~ 0.3 using single-component Ti_3C_2 MXene water dispersion, which is higher than the previously reported GO-based system [7, 8]. Several recent publications found certain water-based dispersions containing MXene additives have excellent tribological performance [8, 12, 37] and can even trigger superlubricity at the macroscale [38]. A common feature among these studies is the use of a second additive other than the MXene.

In short, our literature survey appears to suggest the lubricity of MXene is best harnessed when used alongside other additives. As an example, Lian et al. [39] fabricated a composite MXene/GO solid lubricant coating with significantly improved friction and wear environmental insensitivity as compared to GO coating, possibly due to improved tribofilm stability induced by MXene. Similar result is reported recently by Miao et al. [40]. However, in both studies, limited insight on the mechanistic synergy between MXene and GO was provided. The primary aim of this study, therefore, is to further elucidate the possible synergistic lubrication mechanism of MXene/GO. The secondary aim, is to test the potential of MXene/GO as a water-based boundary lubricant additive. Tribological experiments were designed to compare lubricity of water-based dispersions of $Ti_3C_2T_x$ MXene, GO, and MXene/GO. Focused ion beam microscopy, *in-situ* contact observation and atomic force microscopy (AFM) based adhesion measurements were further conducted to study tribofilm stability and structure. A proposed synergistic lubrication mechanism was finally given based on new insights gained in this study.

2 Experimental

2.1 Preparation of $Ti_3C_2T_x$ MXene

$Ti_3C_2T_x$ MXene was obtained by selective etching of the Al atomic layers from a Ti_3AlC_2 MAX precursor (1–40 μm particle size, XFNANO Materials Tech Co., Ltd.). The particle size distribution of Ti_3AlC_2 MAX precursor measured using a laser diffraction instrument (Malvern Mastersizer 2000, Malvern, UK) is shown in Fig. 1(a). 1 g of MAX precursor was slowly added to 20 mL of hydrofluoric acid (HF, 10%, ACROS) while stirring with a Teflon magnetic stir bar. The reaction was allowed to proceed for 24 h at room temperature. Then, the solution was washed by repeated centrifugation (3,500 rpm for 5 min) to obtain $Ti_3C_2T_x$ and decanted using deionized water until the pH > 6. To confirm the MXene's mass fraction and structural characteristic, the resulting dispersion was filtered and vacuum dried for 36 h at 40 °C.

2.2 Preparation of GO dispersions and MXene/GO dispersions

GO was fabricated from graphite powder using a modified Hummer's method [10, 41]. In an ice bath environment, graphite powder (0.65 g, ~ 40 μm, ACROS), and sodium nitrate (0.5 g) were added to sulfuric acid (50 mL, 98 wt%). The particle size distribution of graphite powder is shown in Fig. 1(b)
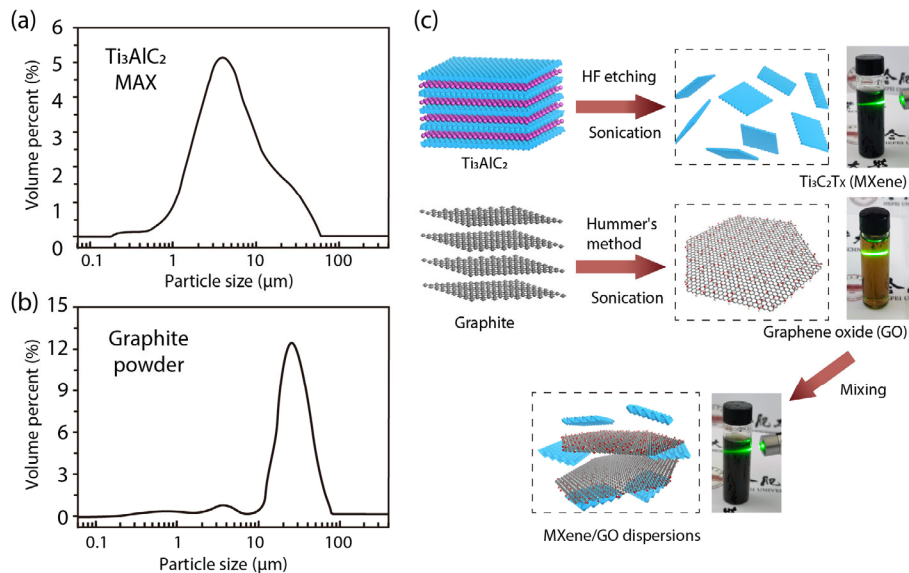
Fig. 1 Particle size distributions of (a) Ti_3AlC_2 MAX precursor and (b) graphite powder. (c) Schematic description of the fabrication process for $Ti_3C_2T_x$ (MXene), graphene oxide (GO), and MXene/GO dispersions.

suggesting a slightly larger size than that of the Ti_3AlC_2 MAX precursor. Potassium permanganate (3 g) was slowly immersed into the solution and stirred at 36 °C for 12 h. Then, the solution was re-dispersed using deionized water (70 mL) and mixed with H_2O_2 solution (3 mL, 30%) to produce a bright yellow suspension. The mixture was then centrifuged and washed with deionized water to remove the remnant salt and acid. The resulting dispersion was filtered under vacuum conditions and dried for 36 h under vacuum and at 40 °C.

Figure 1(c) displays the fabrication processes of the MXene (1.0 mg/mL), GO (1.0 mg/mL), and MXene/GO dispersions (0.5/0.5 mg/mL) in this study. Their digital images were obtained after a three-week placement and showed good stability over the period. The images identified the Tyndall scattering effect in the colloidal solutions of MXene, GO, and MXene/GO by passing a green beam through the aqueous dispersions.

2.3 Characterization

As-synthesized MXene and GO were characterized by high-resolution transmission electron microscopy (HR-TEM, JEM-2100F, JEOL) using an acceleration voltage of 200 keV. Atomic force microscopy (AFM) and X-ray photoelectron spectroscopy (XPS; ESCALAB 250Xi, Thermo Fisher Scientific, USA) were used to characterize the morphological and chemical

characteristics of the samples. Phase analyses were performed using X-ray diffraction in a powder diffractometer (X-Pert PRO MPD, PANalytical) and Raman spectroscopy (HR-800, Horiba, 532 nm laser excitation). Sample specific surface areas were measured by nitrogen adsorption/desorption at –196 °C using a Quantachrome Autosorb-iQ3 automated gas adsorption system and calculated based on the Brunauer–Emmett–Teller (BET) method. Particle size measurements of the MXene and GO through dynamic light scattering (DLS) and the Zeta potentials were obtained using a Zeta potential analyzer with a 633 nm laser source (Zetasizer Nano ZS90, Malvern). Viscosities of DI-water and typical dispersion samples were measured using an NDJ-79 type rotational viscometer by measuring the torque required to rotate the bob in the tested fluid at a shear rate of 100 s^{-1}.

2.4 Experimental apparatus and measurements

Tribological performances of lubricants were investigated using a customized surface force apparatus (SFA, Fig. 2) in reciprocating mode with a stroke length of 2 mm. Our previous reports provide detailed information on this SFA [42, 43]. A linear-motor stage (PI/V-408.132020) with a resolution of 20 nm provided the linear reciprocating motion of the bottom plate. The top quartz glass plate was mounted on a four-beam structured cantilever flexure. A 250 μm piezo-stage
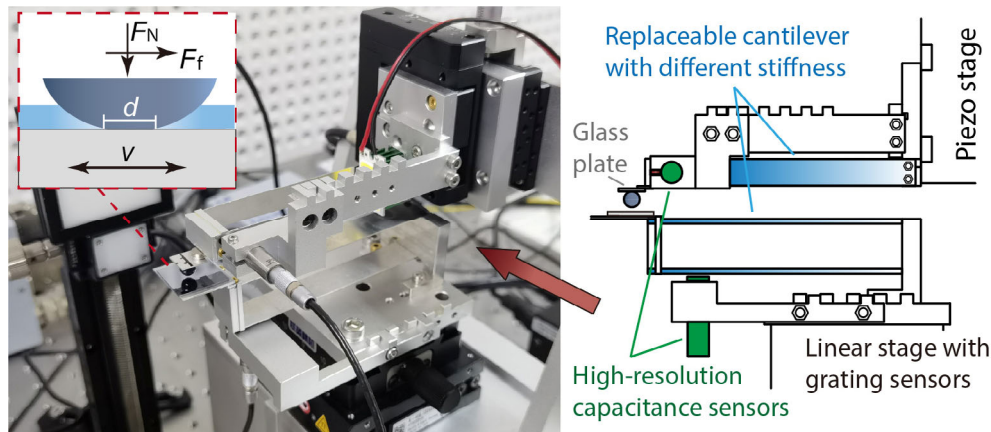
Fig. 2 Digital image and schematic of SFA.

(PI/P-622.1CD) provided vertical adjustment of the top assembly with a resolution of 0.7 nm. Vertical and lateral shifts of the cantilevers were measured with two high-resolution capacitance sensors (±1 nm, PI/E-E01.001) to quantify normal and lateral forces at the contact.

The standard test condition was set with a linear sliding speed of 0.5 mm/s, a normal load of 5 mN (corresponding to a Hertzian contact pressure of ~ 140 MPa), and a test duration of 2 h (total of 720 cycles). The resolutions of friction (lateral force) and load (normal force) measurements are 0.01 mN at the applied force of 0.1–500 mN. Constant velocity tests were conducted at 0.5 mm/s with applied normal loads in the range of 0.1–500 mN (63–210 MPa). Constant load tests were conducted at 5 mN with varying velocities of 0.02–10 mm/s. Friction data within the middle 60% of the wear track was used to extract the average friction coefficient per cycle using the method proposed by Burris and Sawyer [44]. Each test was repeated at least five times. During the tests, the laboratory temperature and humidity are constantly controlled at ~ 25 °C and 40% RH, respectively.

The tribopairs consist of 6 mm diameter silicon nitride (Si_3N_4) balls prepared by the high-temperature sintering method, and P-Si (111) single crystal silicon wafers (Si, 10 mm × 10 mm) produced via the Czochralski method. The elastic modulus of the Si_3N_4 and Si samples are 320 and 190 GPa, respectively, and the Poisson's ratios are 0.26 and 0.28, respectively. The Vickers hardness of the Si_3N_4 ball is ~ 35 GPa [45], which is higher than that of the Si countersample

(~ 11 GPa) [46]. The root-mean-square (RMS) roughness of the plate and the ball samples were 10 and 50 nm, respectively. Prior to the tests, the tribopairs were ultrasonically cleaned in acetone and ethanol for 15 min and dried at 80 °C. The silicon wafer was placed on a custom culture dish with a diameter of 20 mm and immersed with 800 μl of lubricants. The volume of lubricant was selected to best limit any meniscus effect. To confirm the lubrication regime, Dowson–Hamrock's minimum film thickness theory was used [47]. The maximum film thicknesses were calculated to be ~ 0.85 nm for all test groups corresponding the film thickness ratio of ~ 0.0139, which indicates that all test groups were under the boundary lubricating condition.

2.5 Analysis of wear tracks

After the tribological tests, tribopairs were washed using DI-water and vacuum dried for 2 h at 40 °C for better observation of the contact regime. Morphological and chemical characterization was performed using 3D laser scanning confocal microscopy (VK-X100, Keyence), Raman spectroscopy (HR-800, Horiba, 532 nm laser excitation), XPS (ESCALAB 250Xi, Thermo Fisher Scientific), focused ion beam microscopy (FIB, Helios NanoLab 600i, FEI) combined with scanning electron microscopy (SEM), and HR-TEM (HR-TEM, JEM-2100F, JEOL).

2.6 Adhesion measurements

AFM (Bruker Nano Caliber™) was used to evaluate the difference between $Ti_3C_2T_x$ MXene, GO, and

MXene/GO nanocomposite samples in their adhesive ability. A typical force versus displacement response for tip approach and withdrawal measured on the sample is shown in Fig. 3(a), including tip approaching (i), "jump-in" phenomenon (ii), pre-loading and withdrawing (iii), "jumps-off" phenomenon (iv), and separation (v). The adhesion energy was calculated from the measured "jump-off" (or maximum adhesion) force using the Maugis–Dugdale theory [48]:

$$W_{adh} = \frac{F_{adh}}{\lambda \pi R_{tip}} \qquad (1)$$

where W_{adh} is the adhesion energy per unit area, F_{adh} is the maximum adhesion force measured during the withdrawal stage, R_{tip} is the tip radius (~ 40 nm, according to Fig. 3(b)) and λ is an effective coefficient of 1.60 [49]. To account for the roughness effect, the tip RMS roughness, σ_{tip} (~ 0.2 nm provided by the vendor), and the average surface roughness of the measured area were employed using the modified Rumpf model [48]. The calculated adhesion energy is

$$W_{adh} = \left(\frac{F_{adh}}{\lambda \pi R_{tip}} \right) \frac{\left(1 + \frac{R_{tip}}{1.48\sigma_{surf}}\right)^{-1} + \left(1 + \frac{1.48\sigma_{surf}}{Z_0}\right)^{-2}}{\left(1 + \frac{R_{tip}}{1.48\sigma_{tip}}\right)^{-1} + \left(1 + \frac{1.48\sigma_{tip}}{Z_0}\right)^{-2}} \qquad (2)$$

where σ_{surf} is the RMS roughness of the sample surface, σ_{tip} is the RMS value for the tip, and Z_0 is the equilibrium separation of two surfaces, which was estimated to be 0.3 nm [49]. All adhesion energies in this work were calculated using Eq. (2). The Mica adhesion energy measured by this method is ~ 225.78 mJ/m^2, which is close to the reported values in previous studies [50]. Before the indentations, the morphology of the measured area was obtained to ensure that the RMS roughness of each indentation site are close. The highest applied loads were 20 nN. The load–hold–unload test cycle was 5.0–10.0–5.0 s for each test. The pull-off force was directly measured from the load–displacement plot, and each presented result is averaged from 5 independent measurements. In each measurement interval, the AFM probe was cleaned using acetone to remove potential surface contamination. Figure 3(b) shows that the AFM indentation experiment did not significantly change the curvature of the probe. Thus, the adhesion results measured with the same probe are comparable. During the tests, laboratory temperature and humidity are constantly controlled at 25 °C and 40% RH, respectively.

4 Results and discussion

3.1 MXene, GO, and MXene/GO nanostructures

We first investigated the nanostructures of graphene oxide (GO), $Ti_3C_2T_x$ (MXene), $Ti_3C_2T_x$ MXene/GO (MXene/GO) as described before. TEM and selected area electron diffraction (SAED) revealed the polycrystalline nature of the $Ti_3C_2T_x$ MXene as shown in Fig. 4(a). HR-TEM further verified the layered structure of MXene with an interlamellar spacing of ~ 0.9 nm. Figure 4(b) illustrates the 2D characteristic and amorphous state of the GO with poor-defined
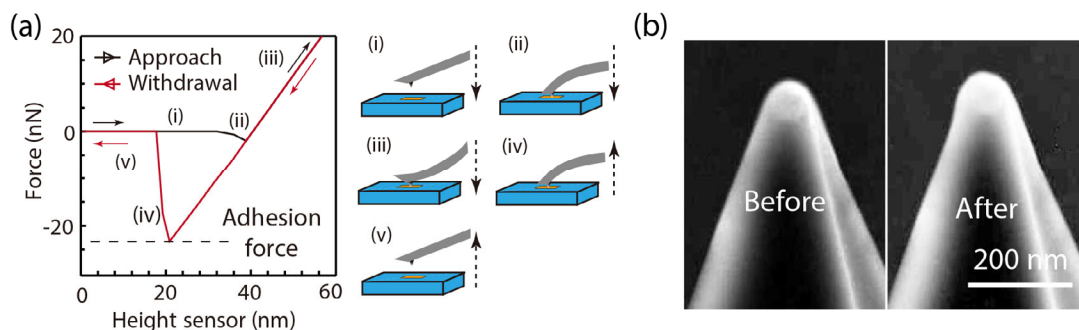

Fig. 3 (a) Force versus displacement graphs: a typical approach and withdrawal curve and cartoons illustrating relative positions of the tip and the sample during different key stages of the AFM indentation process. (b) SEM images of the AFM probe tip before and after the indentation tests.

diffraction rings, which suggests there are defects in the GO nanosheets. Diffraction rings in Fig. 4(c) inset reveal that the selected area contains both the $Ti_3C_2T_x$ and GO nanosheets. The energy dispersive spectroscopy (EDS) elemental mappings suggest that the darker area in the TEM image is mainly $Ti_3C_2T_x$ MXene, and the carbon-rich area contains GO nanosheets. $Ti_3C_2T_x$ nanoflakes are possibly embedded on the GO surfaces in the mixed MXene/GO dispersions. AFM images of the $Ti_3C_2T_x$, GO, and MXene/GO samples after ultrasonication are shown in Figs. 4(f)–4(h), respectively. The average thicknesses of the $Ti_3C_2T_x$ and GO flakes are approximately 6.4 and 1.6 nm. This suggests that the $Ti_3C_2T_x$ MXene nanosheets are mainly few-layer [51], and GO nanosheets are mainly single-layer [11]. The typical size of the GO nanoflake is obviously larger than that of the $Ti_3C_2T_x$ MXene, which is related to the different sizes of their precursors as shown in Figs. 1(a) and 1(b). The MXene/GO image shows a layered structure of the MXene flake on top of the GO, which is consistent with the TEM observations.

XPS was used to analyze the functional groups of GO and MXene samples. Figure 5(a) indicates that there is existence of oxygen-containing functional groups in both nanosheets. Previous studies suggest that these oxygen-containing functional groups can enable MXene and GO to be readily dispersed in water [7, 52]. The oxygen contents of GO were due to the oxidation during the synthesis process, while the fluorine content in $Ti_3C_2T_x$ MXene was mainly introduced from the HF-etching process [53, 54]. X-ray diffraction (XRD) identified nanosheets' structures, as shown in Fig. 5(b). The XRD patterns of GO and MXene have strong diffraction peaks at $2\theta = 6.9°$ and $9.8°$ corresponding to lattice spacings of 1.28 and 0.90 nm, respectively. This indicates that GO and $Ti_3C_2T_x$ MXene sheets have been exfoliated from their precursors [55, 56]. Raman spectra also confirmed they were successfully fabricated (Fig. 5(c)) [38]. The region 230–470 cm^{-1} represents in-plane vibrations of surface groups attached to titanium atoms responsible for the hydrophilicity of $Ti_3C_2T_x$ MXene sheets [57].
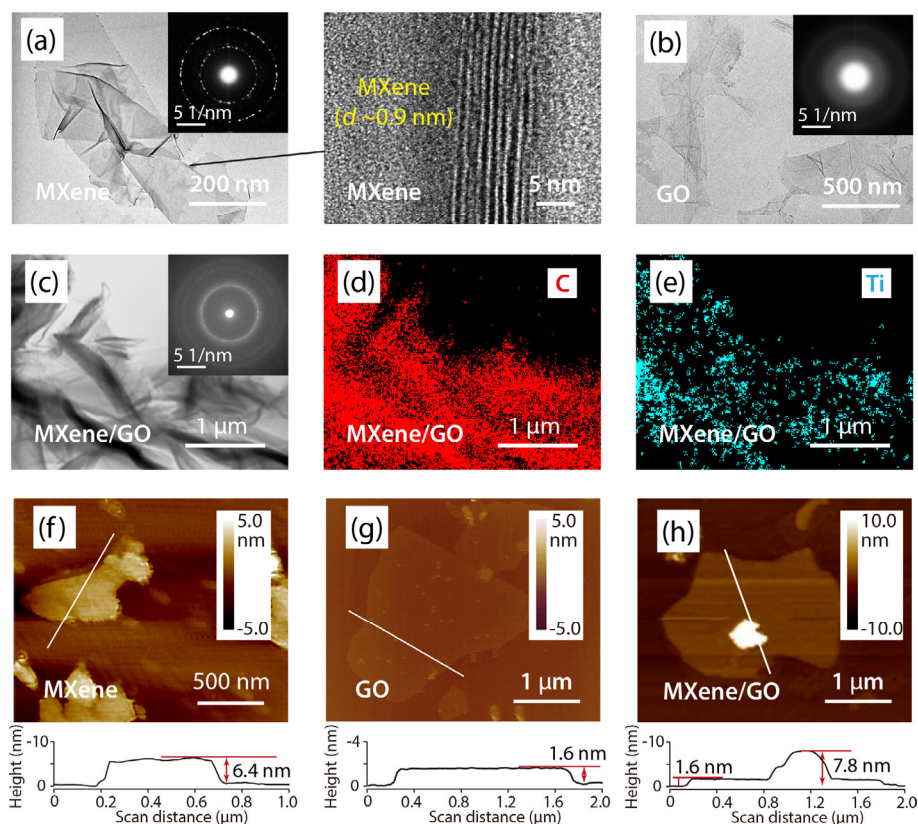

Fig. 4 TEM images of (a) MXene, (b) GO, and (c) MXene/GO. The insets show their corresponding diffraction patterns. EDS elemental mappings of (d) carbon and (e) titanium corresponding to Fig. 4(c). AFM images of (f) MXene, (g) GO, and (h) MXene/GO nanocomposite samples laid onto the mica substrates. The bottom profile corresponds to the white line scan for each AFM image.
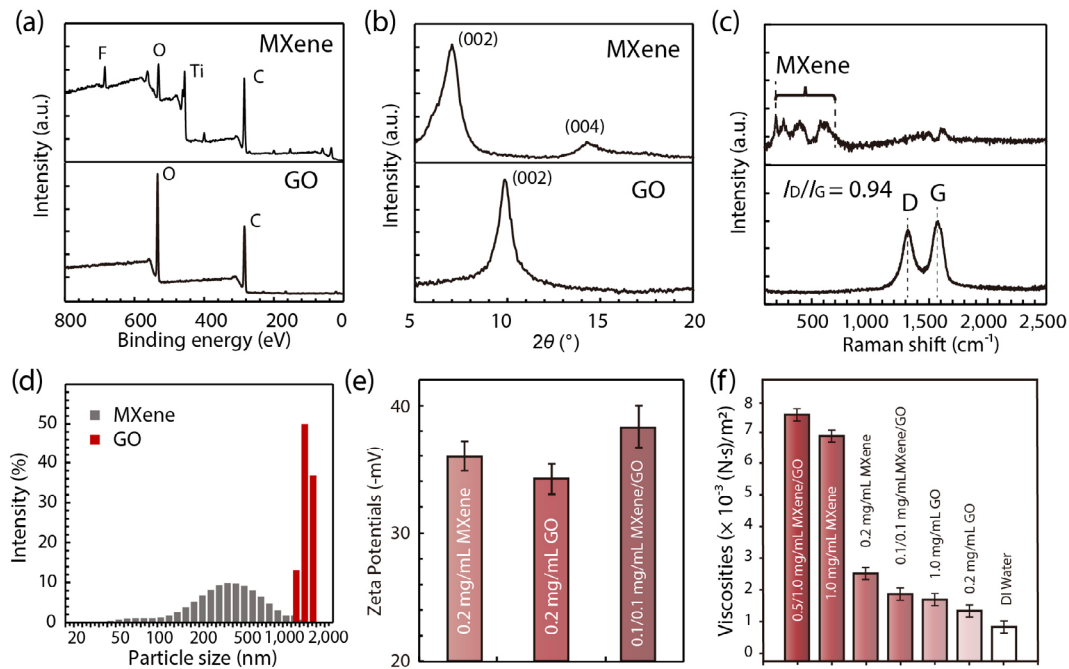
Fig. 5 (a) XPS survey scan spectra, (b) XRD, (c) Raman spectra, and (d) size distribution of MXene and GO nanosheets. (e) Zeta potentials of the dispersions of MXene, GO, and MXene/GO. (f) Viscosities of DI-water and typical GO, MXene, and MXene/GO dispersions.

The average size of $Ti_3C_2T_x$ is approximately 422 nm, which is relatively smaller than that of GO (~ 1,423 nm), as shown in Fig. 5(d). This is consistent with the AFM images. The Zeta potentials of MXene, GO, and MXene/GO dispersions were –35.3, –33.9, and –38.1 mV, respectively (Fig. 5(e)). This indicates that the additional use of MXene is unlikely to affect the GO's stability in water. Viscosities of DI-water and typical GO, MXene, and MXene/GO dispersions were measured at a shearing rate of 100 s^{-1} (Fig. 5(f)). Although the viscosity of mono-dispersed MXene is slightly higher than that of GO with the same concentration, adding 0.1 mg/mL MXene in 0.1 mg/mL GO dispersion did not significantly increase the dispersion viscosity.

3.2 Tribological performance

Tribological performance of the MXene, GO, MXene/GO composite dispersions, and the reference DI-water was tested with an applied normal load of 5 mN and sliding velocity of 0.5 mm/s for 2 h. It can be observed that MXene partially enhances the friction-reducing ability of pure water. The friction coefficient reached a minimum of ~ 0.24 at 0.2 mg/mL

(Fig. 6(a)), then increased with higher MXene concentrations. The lubricity of GO additives at a sufficient concentration (0.05–1.0 mg/mL) is better than that of the MXene. For example, the average friction coefficient of the 0.2 mg/mL GO is ~ 0.095 (Fig. 6(b)), almost a third of the comparable MXene dispersion. This suggests that the hydrophilicity alone of 2D nanomaterials is insufficient to enable them as good water-based lubricant additives. GO nanoflakes are with certain characteristics enabling them to exhibit better friction-reducing performance than $Ti_3C_2T_x$ MXene does.

As expected, the synergistic use of MXene and GO in water demonstrates a more pronounced friction-reducing effect than that of single-component MXene or GO (Fig. 6(c)). This effect shares similarities with several studies using GO composites [14, 58, 59]. With the additional use of 0.1 mg/mL MXene additive, the GO dispersion (0.1 mg/mL) achieved a 4-fold enhanced lubricative performance, that is, the friction coefficient reduced from 0.090 to 0.021. However, the tribological performance of MXene/GO samples seems to worsen with further addition of MXene. This could be related to the greatly increased viscosities with the increased MXene concentration as shown in Fig. 5(f). At low
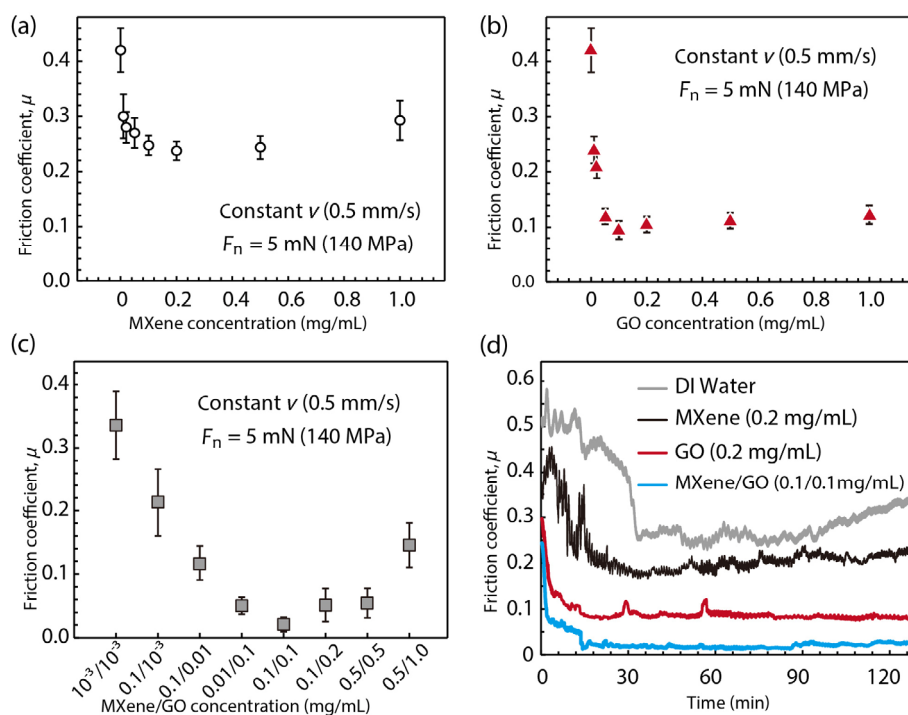
Fig. 6 Friction coefficient as a function of concentration for (a) MXene, (b) GO, and (c) MXene/GO composite dispersions. Each data point represents the average of 5 individual repeats, and error bars represent the 95 % confidence interval. (d) Temporal evolution of the friction coefficients during the tribological tests of MXene (0.2 mg/mL), GO (0.2 mg/mL), MXene/GO (0.1/0.1 mg/mL) samples, and DI-water.

MXene concentration (< 0.5 mg/mL), the tribological performance of the MXene/GO dispersions confirmed our previous hypothesis: the use of MXene additives can additionally improve the lubricating functionality of aqueous GO dispersions through a synergistic effect. The underlying mechanisms will be investigated hereafter.

To investigate the running-in behaviors of tested samples, temporal evolutions of the friction coefficients during the tests are plotted in Fig. 6(d). The friction coefficient evolution of the DI-water reference group has an obvious running-in behavior for lubricated contacts. The friction coefficient gradually decreased during the initial 30 min sliding likely due to the formation of a hydroxylated film on the Si_3N_4 surface [60]. After 30 min of sliding, the removal of silicon oxides, direct contact, and wear led to increased friction [58]. The running-in behavior of the aqueous MXene dispersion is similar to that of DI-water with a relatively lower friction coefficient indicating that MXene nanosheets can partially reduce the interfacial friction. The GO and MXene/GO samples demonstrate much lower friction coefficients with a shorter

running-in. Notably, the GO and MXene/GO samples show some frictional fluctuations around the low base level after 30-min sliding. This indicates dynamic processes near the lubricated interface potentially involving the degradation and recovery of the low-friction, nanosheet agglomeration, and tribolayer formation [61].

The sensitivities of the three types of lubricant to varying loads or velocities were further investigated. Figure 7(a) shows the average friction coefficients of MXene (0.2 mg/mL), GO (0.2 mg/mL), MXene/GO (0.1/0.1 mg/mL) at the normal load of 0.1 mN were ~ 0.36, 0.32, and 0.22, respectively, which are both higher than the performances at the load of 5 mN. This effect can be understood as "adhesion-controlled" friction, where the friction force is increasingly related to surface adhesion under lower contact pressures [62, 63]. For example, friction forces measured in the MXene/GO lubricated tribosystem are nonlinear to the normal load in 0.05–1.0 mN (Fig. 7(b)). The friction coefficient shows no obvious change for each test group when the applied load is in the range of 1.0–10 mN, demonstrating the "load-controlled" friction
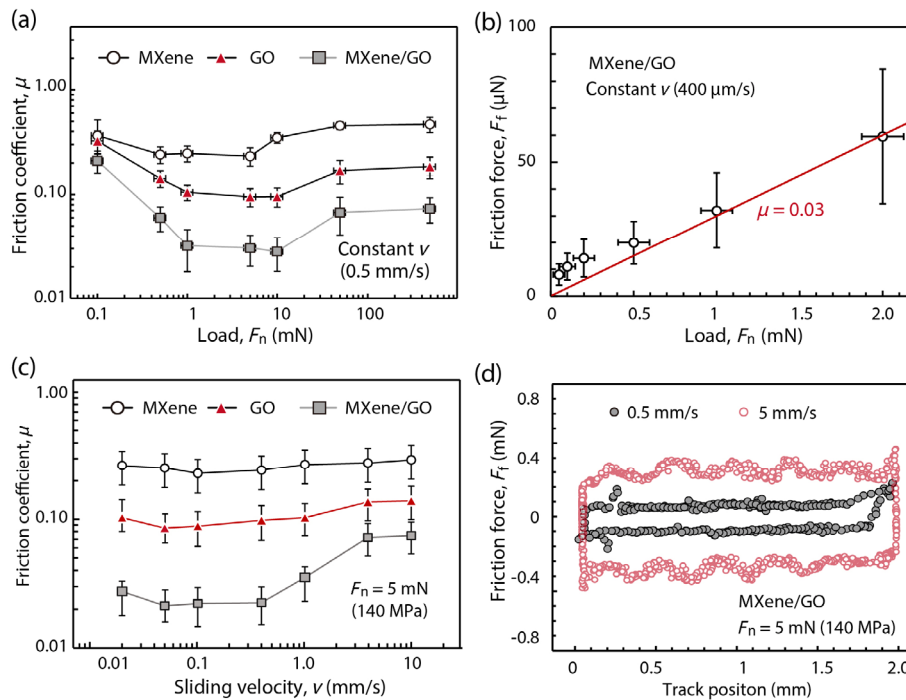
Fig. 7 (a) Average friction coefficients of MXene, GO, and MXene/GO samples plotted as a function of the normal load. (b) Friction forces as a function of the average load for the 0.1/0.1 mg/mL MXene/GO. The red line represents the friction linear to the normal load when the coefficient of friction is 0.03, which is used to compare the experimental results. (c) Average friction coefficients plotted as a function of sliding velocity for MXene, GO, and MXene/GO samples. Each data point represents the average of 5 individual repeats, and error bars represent the 95 % confidence interval. (d) Steady-state friction loops at two sliding velocities for the 0.1/0.1 mg/mL MXene/GO.

at a relatively higher contact pressure, then transits to a higher level when the applied load is larger than 50 mN. The frictional transition behavior was suspected to be related to the wear of countersamples, which will be investigated in the following sections.

The effects of sliding velocity on frictional behavior were also investigated. At the velocity range of 0.01–1.0 mm/s, the three tribo-systems exhibited stable frictional behaviors with friction coefficients around 0.25, 0.10, and 0.04, respectively (Fig. 7(c)). At higher velocities (> 5.0 mm/s), an increase was observed for the MXene/GO sample. Typical friction loops (i.e., friction force versus wear track position) were plotted in Fig. 7(d). At a velocity of 0.5 mm/s, the measured friction force was about 0.10 mN during sliding; while the lateral force measured in the tribo-system was approximately 0.34 mN at a velocity of 5.0 mm/s, a nearly 3-fold higher friction increase. For the constant velocity regions, the fluctuations of friction loops at 5 mm/s are more pronounced than that at 0.5 mm/s. Since the frictional behavior under

boundary lubrication is closely related to adsorption film behaviors at the microscale [64]. We suspect that the transition from the low friction zone to relatively higher friction is related to the wear of the countersample.

3.3 Wear track observations

Wear tracks were analyzed for the DI-water reference, MXene (0.2 mg/mL), GO (0.2 mg/mL), and MXene/GO (0.1/0.1 mg/mL) lubricated countersamples. These wear tracks were obtained after 2 h of the reciprocation sliding. In the case of the contact pressure of ~ 140 MPa and sliding speed of 0.5 mm/s, the optical and laser-scanning height images show an obvious wear track formed on the DI-water reference sample with a width of ~ 18.2 μm (Fig. 8(a)). The width of the wear tracks was ~ 14.6, 13.7, and 12.9 μm for the 0.2 mg/mL MXene, 0.2 mg/mL GO, and 0.1/0.1 mg/mL MXene/GO dispersions, respectively (Figs. 8(b)–8(d)). The height profile line scans of GO and MXene/GO lubricated countersamples show no obvious material sacrificing
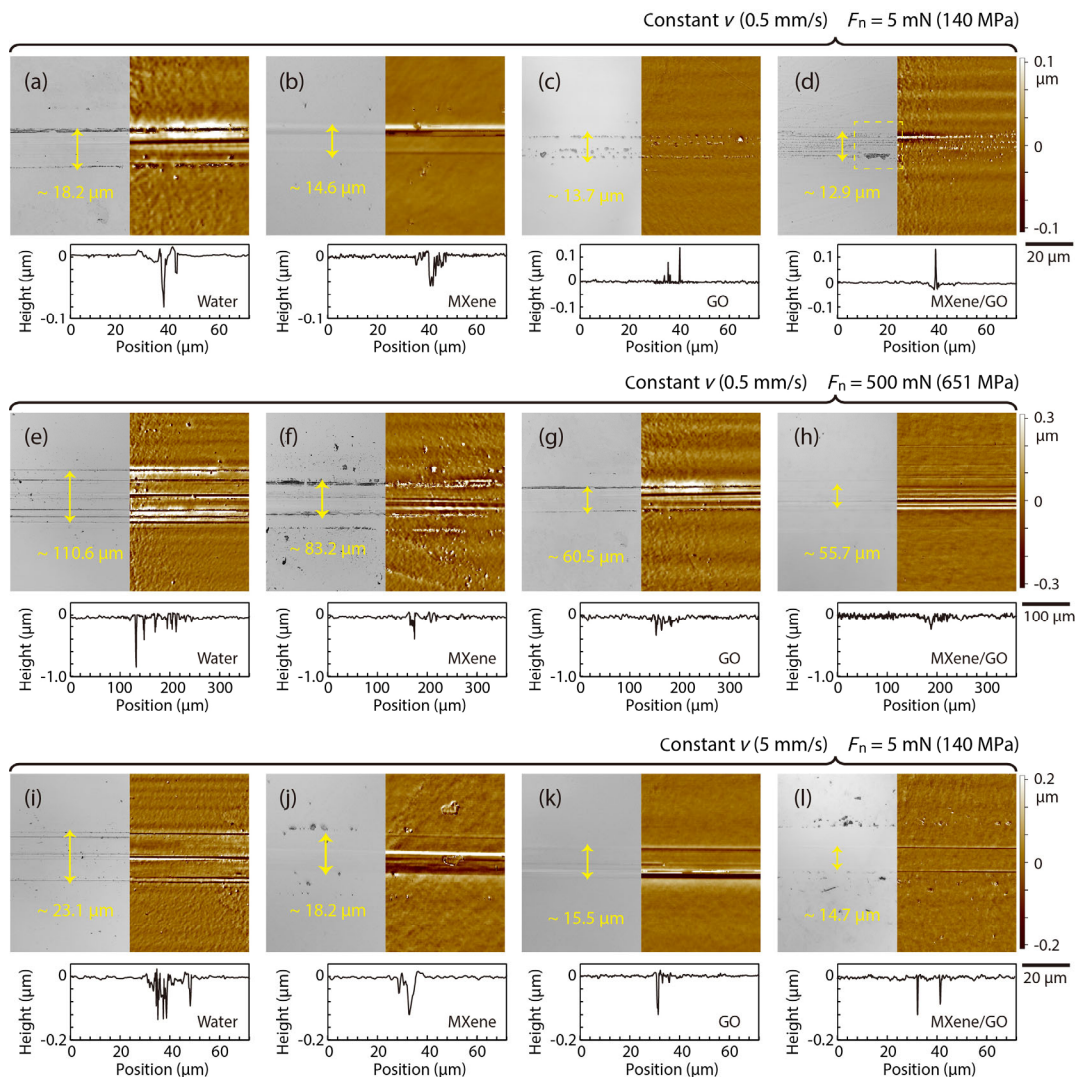
Fig. 8 Optical micrographs (left) and laser-scanning height imaging (right) of the resulting wear features of the counterfaces when lubricated by (a) DI-water, (b) 0.2 mg/mL MXene, (c) 0.2 mg/mL GO, and (d) 0.1/0.1 mg/mL MXene/GO at the applied load of 5 mN with velocity of 0.5mm/s. Wear track morphology lubricated by (e) DI-water, (f) MXene, (g) GO, and (h) MXene/GO samples at the applied normal load of 500 mN and sliding velocity of 0.5mm/s. Wear track morphology lubricated by (i) DI-water, (j) MXene, (k) GO, and (l) MXene/GO samples at the applied load of 5 mN and sliding velocity of 5.0 mm/s.

but adsorption film residues onto their surfaces; whereas obvious abrasions occur on the counterface lubricated by the 0.2 mg/mL MXene. It is suspected that MXene formed a less protective adsorption film than GO or MXene/GO did.

The increase of applied load or sliding velocity likely led to severer wear of the counterface. In cases with a relatively higher applied load (500 mN), the maximum wear track depth of DI-water- and MXene-lubricated counterface is approximately 0.9 and 0.4 μm (Figs. 8(e) and 8(f)), respectively. The worn countersamples lubricated by GO, and MXene/GO

dispersions also have noticeable abrasive marks on their surface (Figs. 8(g) and 8(h)). In the cases tested with the sliding velocity of 5 mm/s, the worn counterfaces of DI-water, MXene, GO, and MXene/GO test groups are with maximum wear track depth of approximately 0.15 and 0.12, 0.10, and 0.09 μm respectively (Figs. 8(i)–8(l)). These results suggest that the excessive normal load (> 500 mN) or sliding velocity (> 5 mm/s) tends to induce an increase in counterface abrasion, which is responsible for the frictional transition behaviors shown in Figs. 7(a) and 7(c).

To understand the synergistic effect of the MXene/GO, we further analyzed the Si$_3$N$_4$/Si tribopairs' surfaces lubricated by 0.1/0.1 mg/mL MXene/GO at the applied load of 5 mN and sliding velocity of 0.5 mm/s. Three-dimensional characterization confirmed that the countersample was with no obvious abrasion but an adsorption film (Fig. 9(a)). High-resolution XPS measurements show the C–C peak at 284.6 eV and the C–Ti peak at 281.7 eV in the C 1s spectrum. The Ti^{2+} and Ti^{3+} peaks in the Ti 2p spectrum are ascribed to typical signals of the structural Ti–C bonding and the surface C–Ti–T$_x$ bonding [19]. It is demonstrated that there is no significant chemical change for nanoflakes adsorbed on the counterface, thus enabling them to lubricate the contact surfaces with their intrinsic low shear strength.

Morphology measurement shows that the Si$_3$N$_4$ sample has an obvious adsorption film formed on its surface as shown in Fig. 9(d). XPS measurements confirmed the oxidation of MXenes with a reduced intensity of C–Ti–T$_x$ bonds (Fig. 9(e)) and a pronounced peak at 458.6 eV in the Ti 2p spectrum (Fig. 9(f)) which corresponds to the newly formed titanium dioxides [19, 65]. This implies stress-induced breakage or degradation of Ti$_2$C$_3$T$_x$ occurring on the Si$_3$N$_4$ surface, which requires further characterizations to determine the tribochemical details.

Cross-sectional microscopy analysis of the wear track using FIB was performed to further identify the MXene/GO tribolayer nanostructure. Figure 10(a) shows that the thickness of the adsorbed MXene/GO layer is approximately 300 nm. TEM characterization of the cross-sectioned adsorbate/substrate interface reveals the adsorption film consisting of MXene and GO flakes (Figs. 10(b) and 10(c)). Moreover, stress-induced deformation and expansion of MXene nanosheets were detected with the increased layer spacings. This indicates that the adsorption film might reduce the interfacial friction through the interlayer slippage of MXene nanosheets. The Ti$_3$C$_2$T$_x$ MXene flakes absorbed onto the silicon surface confirmed our previous hypothesis that GO with a relatively large surface area might help MXene flakes to be retained near the tribo-interface, thus forming a composite tribolayer.

The friction-induced film on the Si$_3$N$_4$ sample has a total thickness of approximately 200 nm (Fig. 10(d)). Although the outermost tribofilm on Si$_3$N$_4$ has a similar nanostructure to that on the counterface (Fig. 10(e)), high-resolution microscopy revealed that the bottom of the tribofilm is mainly amorphous with some titanium dioxide nanocrystals (Fig. 10(f)), which is distinct from the adsorption layer on the counterface. This indicates that stress-induced breakage or tribochemical degradation of Ti$_2$C$_3$T$_x$ nanosheets occurred on the Si$_3$N$_4$ surface during the reciprocating
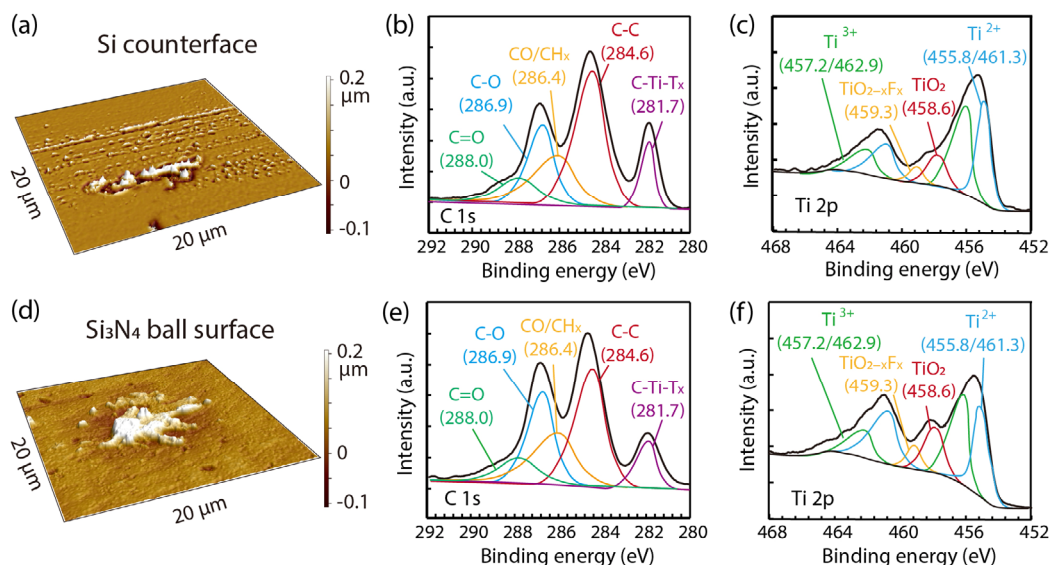

Fig. 9 (a) Three-dimensional characterization, (b) high-resolution spectra of C 1s, and (c) Ti 2p for the adsorption film of the resulting wear features at the Si sample in 0.1/0.1 mg/mL MXene/GO test. (d) Three-dimensional characterization, (e) high-resolution spectra of C 1s, and (f) Ti 2p for the tribofilm formed on the corresponded Si$_3$N$_4$ counterbody.
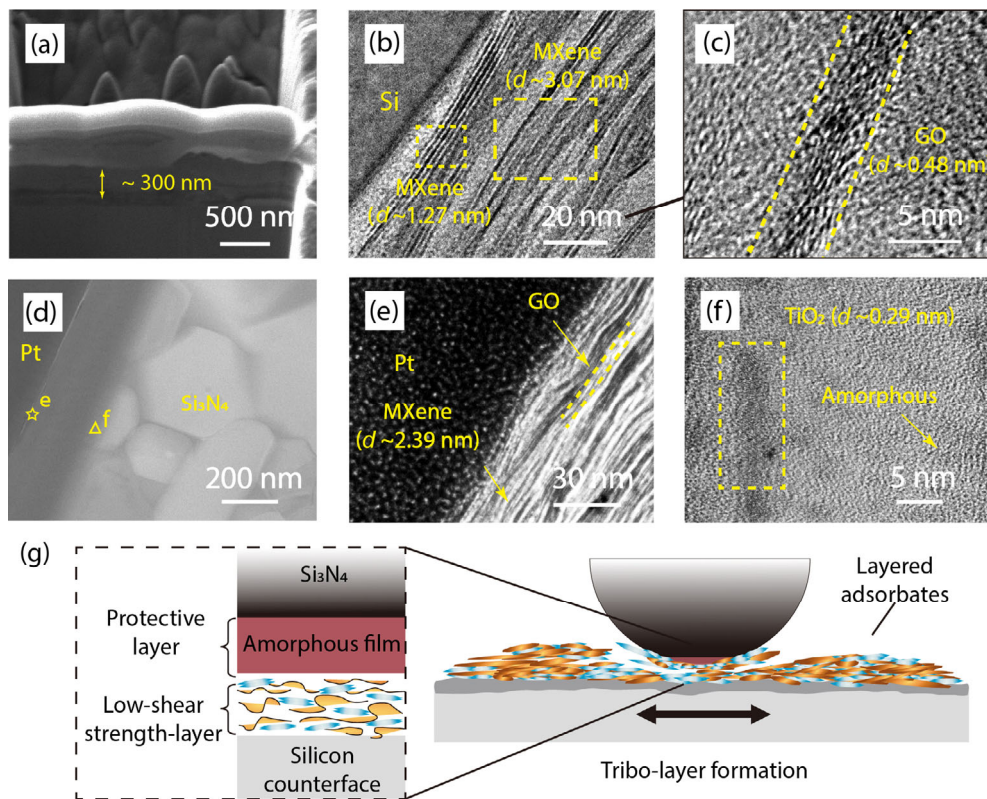
Fig. 10 (a) SEM, (b) TEM, and (c) HR-TEM micrographs of the cross-sectional adsorbates on the wear track of MXene/GO-lubricated counterface. (d) TEM of the cross-sectional tribofilm on Si_3N_4 surface and HR-TEM micrographs at corresponding areas marked with (e) a star and (f) a triangle. (g) Schematic illustration of the MXene/GO tribolayer structures.

sliding [38], which is consistent with the XPS spectra. Combined with the evidence that expanded MXene flakes appeared in the outermost of the tribofilm, it was suspected that the pressure-induced interlayer slippage/exfoliation of MXene flakes enhanced their degradation in the presence of dissolved oxygen as

$$Ti_2C_3 + O_2 \xrightarrow{\text{Thermo/mechanical activation}} TiO_2 + \text{amorphous C} \tag{3}$$
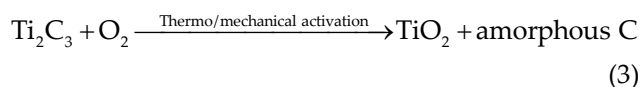
Similar observations have been reported in previous studies [35, 38, 40]. This protective tribofilm and adsorption film on the counterface synergistically reduced the interfacial friction and countersample wear as illustrated in Fig. 10(g), which is derived from nanomaterials' characteristics including the high cohesive ability of GO, interlayer slippery of nanosheets, and protective tribofilms formation due to MXene degradation.

3.4 Lubrication mechanism analyses

To investigate the lubrication mechanisms of MXene,

GO, and MXene/GO dispersions, model experiments were conducted to observe the tribolayer characteristics and stability. A plano-convex glass lens with a probe radius of 6.0 mm and RMS roughness of 5 nm was used to replace the Si_3N_4 ball. The transparency of the lens enables *in-situ* optical microscopy of the tribolayers within the contact zone. Notably, the Si_3N_4 balls were used in previous tests due to the relatively higher hardness of Si_3N_4 than that of silicon counterface; whereas the glass probe has a lower hardness than silicon [66] and might be abraded during sliding leading to complications in wear track analysis. However, we found no noticeable glass probe abrasion in these tests, potentially because of tribofilm formation.

The model experiments were set at 500 mN load, enabling a relatively large contact area for better contact observation. Contact snapshots at 1, 30, and 120 min of experiments were obtained for the SiO_2–Si tribo-interfaces lubricated by 0.2 mg/mL MXene, 0.2 mg/mL GO, and 0.1/0.1 mg/mL MXene/GO and

shown in Fig. 11. Figures 11(a)–11(c) show that the tribolayer (dark area) formed by MXene is unstable with visible abrasion marks on the counterface (Fig. 11(d)). The GO tribolayer was formed after a short running-in with a relatively smaller size than that in the MXene-lubricated system (Figs. 11(e) and 11(f)). Although the break and recovery of the GO tribolayer occurred during the sliding, the total area of the GO tribolayer was smaller than that of the MXene tribolayer (Fig. 11(g)). A smaller contact area of tribolayer can potentially reduce the friction coefficient μ, as [67]:

$$\mu = \frac{F_{\mathrm{f}}}{F_n} \propto \frac{\tau A}{F_n} \tag{4}$$

where F_{f} and F_{n} are friction force and applied load, respectively, τ and A are the shear strength and contact area of the tribolayer. Introducing 2D nanomaterials to construct the tribolayer and increasing the equivalent elastic modulus and hardness of the tribological contact can reduce the friction coefficient by reducing τ and A, respectively [68]. The tribolayer area of the MXene/GO dispersion was even smaller than that of single-component GO dispersion (Figs. 11(i)–11(k)),

which partly explains a better lubricating effect of the MXene/GO. The smaller size of the MXene/GO lubricating layer may be due to the participation of MXene in the construction of the friction layer. Previous studies have found that the mechanical strength of few-layer $Ti_2C_3T_x$ is higher than that of single-layer GO [69]. We postulate that the inclusion of the few-layer MXene nanoflakes in the adsorption film can improve its load-carrying ability. In addition, the XPS and TEM analyses suggest that $Ti_2C_3T_x$ MXene might mechanochemically form amorphous tribofilms during the sliding, which is partially responsible for the improved stability of tribolayer.

The model experiments revealed that the use of GO is beneficial to the formation of stable adsorption films near the tribo-interface, which is critical for the tribological performance of water-based lubricants. To investigate the relationship between the nano-additives' adhesive abilities and their friction-reducing performances, AFM adhesion measurements were conducted for the MXene, GO, and MXene/GO nanoflakes corresponding to the sample surfaces shown in Figs. 4(f)–4(h). The representative force-displacement curves show that the adhesion forces measured on GO, MXene/GO, and MXene samples are approximately
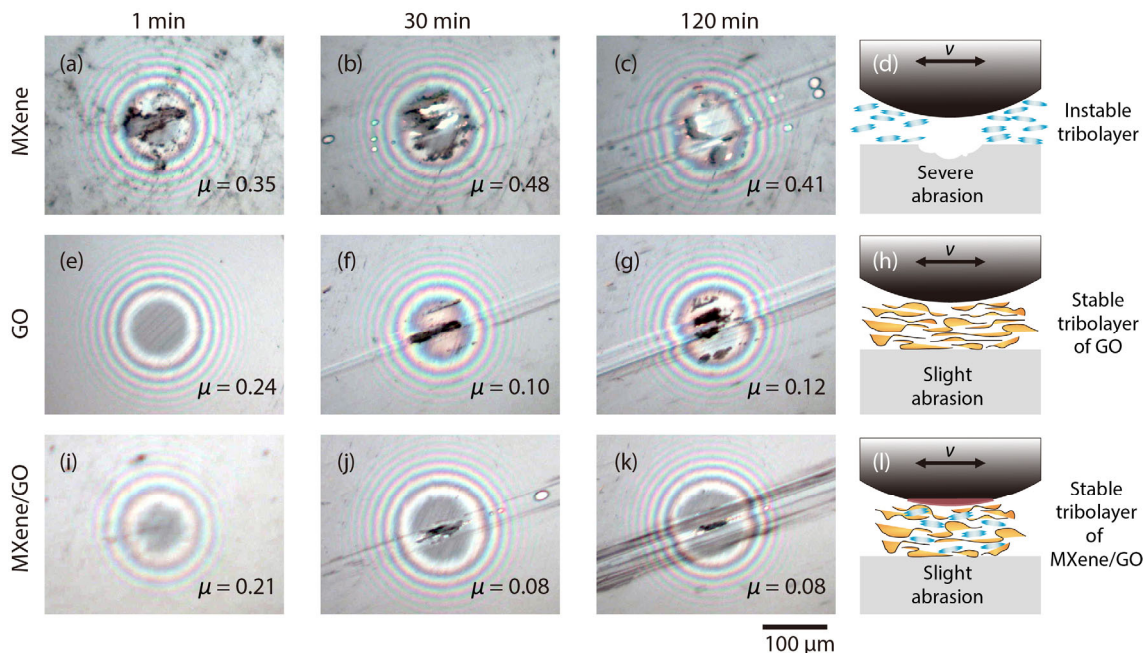
Fig. 11 Captured images of MXene tribolayer (0.2 mg/mL MXene) at (a) 1 min, (b) 30 min, (c) 120 min, and (d) the schematic. Captured images of GO tribolayer (0.2 mg/mL GO) at (e) 1 min, (f) 30 min, (g) 120 min, and (h) the schematic. Captured images of MXene/GO tribolayer (0.1/0.1 mg/mL MXene/GO) at (i) 1 min, (j) 30 min, (k) 120 min, and (l) the schematic.

28.1, 25.5, and 15.2 nN, respectively (Fig. 12(a)). According to Eq. (2), the average adhesion energies of GO and MXene/GO are approximately 182.9 and 140.5 mJ/m^2, both of which are higher than that of the MXene sample (~ 93.46 mJ/m^2, Fig. 12(b)). This supports (1) the relatively higher adhesive ability of GO additives than that of MXene nanoflakes, and (2) the inclusion of GO can help anchor MXene nanosheets to form a layered nanostructured tribolayer as illustrated in Fig. 10(g).

It is suspected that the relatively higher adhesive ability of GO is related to its high specific surface area and oxygen-containing functional groups. Nitrogen adsorption–desorption isotherms show their differences in N$_2$ adsorption ability (Fig. 12(c)). The calculated BET surface area of GO is significantly higher than that of Ti$_3$C$_2$T$_x$ MXene (Table 1). Pore size distributions

assessed by Barrett–Joyner–Halenda method [70] confirm the presence of curvature-induced mesoporous pores at the GO surface (Fig. 12(d)) [13]. A relatively larger surface area of GO nanosheets makes MXene nanoflakes more likely to be adsorbed on tribopairs' surfaces and entangle with nanosheets nearby. Moreover, XPS elemental results reveal that the oxygen content of the GO sample is ~ 33.5%, which is higher than that of Ti$_3$C$_2$T$_x$ MXene. Oxygen/hydroxyl-enriched GO nanoflakes are more likely to interact with tribopairs' surfaces and other nanoflakes through electrostatic interactions, which enables GO to be with high adhesive ability. Tang et al. [71] recently found that GO exhibited stronger surface adhesion in a higher humidity environment. They proposed that water molecules adsorbed by hydroxyl groups play an important role in enhancing the GO's surface
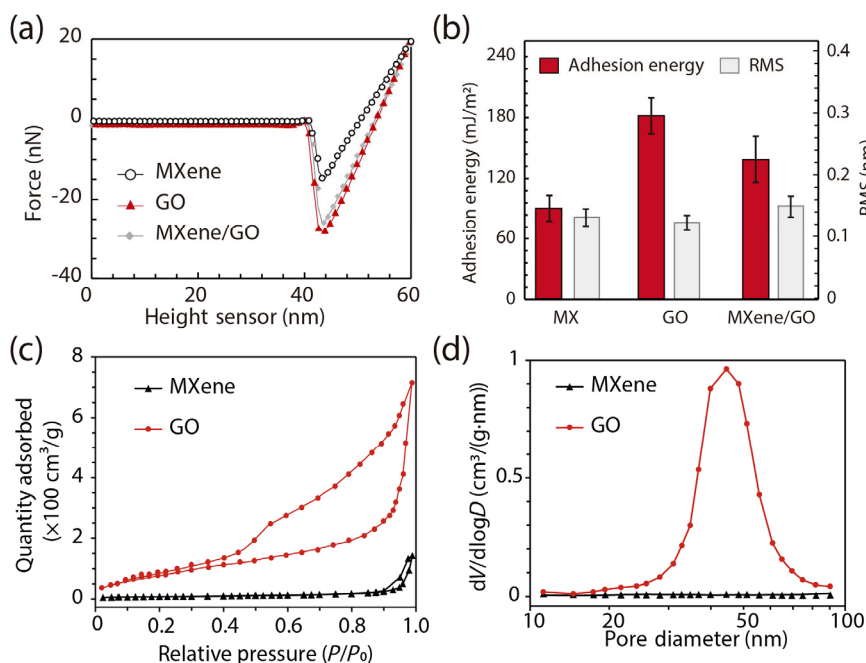

Fig. 12 (a) Representative force–displacement curves measured in the withdrawal processes for Ti$_3$C$_2$T$_x$ MXene, GO, and MXene/GO samples. (b) Average adhesion energies and RMS roughness values for all measured samples with error bars indicating standard deviations. (c) Nitrogen adsorption–desorption isotherms of MXene and GO samples; (d) pore-size distributions calculated using a Barrett–Joyner–Halenda method.

Table 1 Atomic compositions, BET surface area of Ti$_3$C$_2$T$_x$ MXene, GO, and MXene/GO samples. Atomic ratios were obtained from XPS analysis. BET surface areas were calculated based on the BET model using results of nitrogen adsorption/desorption experiments.

—	Carbon content	Fluorine content	Oxygen content	Titanium content	BET surface area (m^2/g)
MXene	34.7%	10.2%	15.2%	40.0%	22.78
GO	66.5%	—	33.5%	—	203.7
MXene/GO	54.4%	5.5%	25.2%	16.9%	96.81

adhesive ability. This further supports the hypothesis that GO with higher oxygen content has higher surface adhesion energy.

Our work demonstrates that the boundary lubrication performance of $Ti_3C_2T_x$ MXene, GO, and MXene/GO dispersions may be strongly related to the adhesion behavior of nanoflakes. It has been revealed that interfacial adhesion behavior is directly affected by contact surface material and roughness [72], and affects various lubricated contacts [64, 73]. We further compared the effects of tribopairs' material and surface roughness on the tribological performance of these lubricants. Ball samples selected include silicon nitride (Si_3N_4), quartz (SiO_2), and 304 stainless steel (304SS) with an average roughness of ~50, 5, and 40 nm, respectively. Countersamples include Si, SiO_2, and 304SS with varying RMS roughness. The applied load and sliding velocity were set to be 5 mN and 0.5 mm/s, respectively. Each test was independently repeated at least three times.

Tribological test results are shown in Fig. 13(a). The lubricating performances of GO and MXene/GO dispersions are generally better than that of MXene. MXene/GO exhibited a synergistic effect in the tests of Si_3N_4/Si(10nm), SiO_2/Si(10nm), and Si_3N_4/SiO_2(5nm) tribo-systems, that is, a statistically significant lower friction coefficient than mono-dispersed GO or MXene. In the cases of using metal or high-roughness samples, the lubricating performance of GO is only slightly higher than that of MXene, and there is no obvious synergic effect in MXene/GO dispersions. This implies that the synergistic effect of MXene/GO is correlated to the lubricating performance that GO exhibited in the tribo-system. The friction coefficients of Si_3N_4/304SS and 304SS/304SS are higher than those using silicon or quartz countersamples, which could be related to the relatively low hardness of 304SS [46, 66, 74]. The friction coefficients corresponding to the left six groups in Fig. 13(a) are plotted against tribopairs' equivalent RMS roughness, σ_{eff} (Fig. 13(b)). The lubricating performances of the three types of lubricants are similar at high roughness. This result indicates that the interfacial adhesion significantly affects the boundary lubrication performance of water-based lubricants using 2D nano-additives.

In summary, the experimental and analysis results revealed the different lubrication mechanisms of MXene and GO additives under boundary lubrication in water. 2D hydrophilic nano-additives do not necessarily create low friction interfaces. The key to achieving a low-friction tribosystem is the formation of a tribolayer with great stability. GO additives with high adhesive ability can (1) improve the stability of the tribolayer by adhering to the counterface, (2) help retain MXene nanoflakes near the tribo-interfaces which could increase the load support capability of the tribolayer. The result is a nanostructured tribolayer with remarkable lubricating functionality, which is responsible for the MXene/GO dispersion's greater lubricity than single-component MXene or GO.
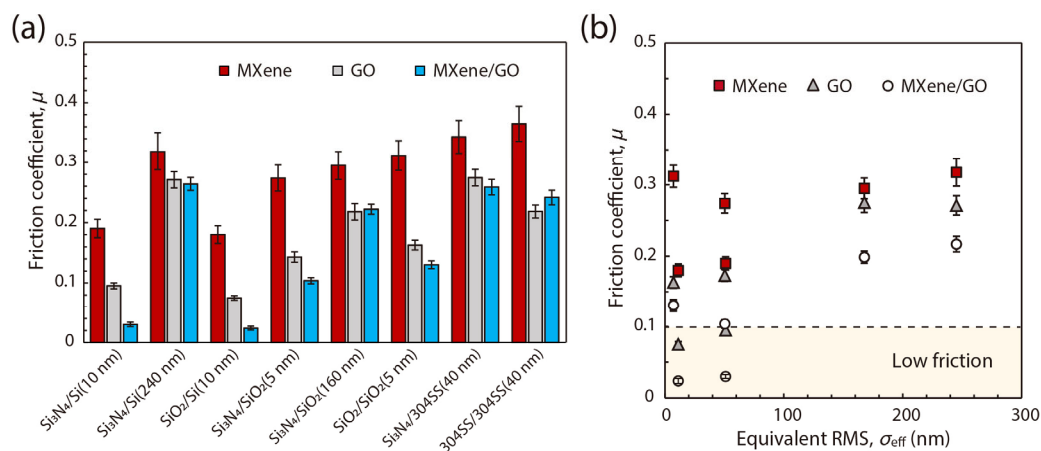

Fig. 13 (a) Friction coefficients of MXene, GO, and MXene/GO samples for selected tribopairs with various RMS roughness. (b) Friction coefficients of MXene, GO, and MXene/GO samples plotted as a function of the RMS roughness of Si and SiO_2 countersamples. Each data point represents the average of 3 individual repeats, and error bars represent the 95% confidence interval.

4   Conclusions

Ti$_3$C$_2$T$_x$ MXene and graphene oxide (GO) have different boundary lubrication performance in water. The lubrication performance of aqueous MXene dispersions is proved to be inferior to that of GO dispersions at the same concentration. Model experiments support that the MXene tribolayer is less stable than that of the GO tribolayer. Atomic force microscopy (AFM) adhesion experiments confirmed that the adhesion energy of GO is higher than that of MXene, which is likely responsible for the better lubricating functionality of GO dispersions.

The mixed MXene/GO lubricant performed significantly better than either the monodispersed GO or MXene with the lowest friction coefficient of ~ 0.021. High-resolution characterizations and model experiments demonstrate that aqueous MXene/GO dispersion synergistically combines the adhesive and cohesive abilities of large-surface-area GO flakes and the mechanical properties of MXene additives to form layered adsorbates and protective tribofilms near the tribo-interface, thus leading to an excellent lubrication functionality.

References

[1]   Berman D, Erdemir A, Sumant A V. Graphene: A new emerging lubricant. *Mater Today* **17**: 31–42 (2014)

[2]   Erdemir A, Ramirez G, Eryilmaz O L, Narayanan B, Liao Y, Kamath G, Sankaranarayanan S K R S. Carbon-based tribofilms from lubricating oils. *Nature* **536**: 67–71 (2016)

[3]   Berman D, Erdemir A, Sumant A V. Approaches for achieving superlubricity in two-dimensional materials. *ACS Nano* **12**: 2122–2137 (2018)

[4]   Wang H, Liu Y. Superlubricity achieved with two-dimensional nano-additives to liquid lubricants. *Friction* **8**(6): 1007–1024 (2020)

[5]   Yu W, Sisi L, Haiyan Y, Jie L. Progress in the functional modification of graphene/graphene oxide: A review. *RSC Adv* **10**: 15328–15345 (2020)

[6]   Liu Y, Li J, Li J, Yi S, Ge X, Zhang X, Luo J. Shear-induced interfacial structural conversion triggers macroscale superlubricity: From black phosphorus nanoflakes to phosphorus oxide. *ACS Appl Mater Interfaces* **13**: 31947–31956 (2021)

[7]   Rosenkranz A, Liu Y, Yang L, Chen L. 2D nano-materials beyond graphene: from synthesis to tribological studies. *Appl Nanosci* **10**: 3353–3388 (2020)

[8]   Marian M, Berman D, Rota A, Jackson R L, Rosenkranz A. Layered 2D nanomaterials to tailor friction and wear in machine elements—A review. *Adv Mater Interfaces* **9**: 2101622 (2021)

[9]   Szabó T, Szeri A, Dékány I. Composite graphitic nanolayers prepared by self-assembly between finely dispersed graphite oxide and a cationic polymer. *Carbon* **43**: 87–94 (2005)

[10]   González-Poggini S, Rosenkranz A, Colet-Lagrille M. Two-dimensional nanomaterials for the removal of pharmaceuticals from wastewater: A critical review. *Processes* **9**: 2160 (2021)

[11]   Kinoshita H, Nishina Y, Alias A A, Fujii M. Tribological properties of monolayer graphene oxide sheets as water-based lubricant additives. *Carbon* **66**: 720–723 (2014)

[12] Ji Z, Zhang L, Xie G, Xu W, Guo D, Luo J, Braham P. Mechanical and tribological properties of nanocomposites incorporated with two-dimensional materials. *Friction* **8**(5): 813–846 (2020)

[13] Suk J W, Piner R D, An J, Ruoff R S. Mechanical properties of monolayer graphene oxide. *ACS Nano* **4**: 6557–6564 (2010)

[14] Ge X, Li J, Luo R, Zhang C, Luo J. Macroscale superlubricity enabled by the synergy effect of graphene-oxide nanoflakes and ethanediol. *ACS Appl Mater Interfaces* **10**: 40863–40870 (2018)

[15] Ghidiu M, Lukatskaya M R, Zhao M Q, Gogotsi Y, Barsoum M W. Conductive two-dimensional titanium carbide 'clay' with high volumetric capacitance. *Nature* **516**: 78–81 (2014)

[16] Naguib M, Kurtoglu M, Presser V, Lu J, Niu J, Heon M, Hultman L, Gogotsi Y, Barsoum M W. Two-dimensional nanocrystals produced by exfoliation of Ti_3AlC_2. *Adv Mater* **23**: 4248–4253 (2011)

[17] Kim S J, Choi J, Maleski K, Hantanasirisakul K, Jung H T, Gogotsi Y, Ahn C W. Interfacial assembly of ultrathin, functional Mxene films. *ACS Appl Mater Interfaces* **11**: 32320–32327 (2019)

[18] Hope M A, Forse A C, Griffith K J, Lukatskaya M R, Ghidiu M, Gogotsi Y, Grey C P. NMR reveals the surface functionalisation of Ti_3C_2 MXene. *Phys Chem Chem Phys* **18**: 5099–5102 (2016)

[19] Halim J, Cook K M., Naguib M, Eklund P, Gogotsi Y, Rosen J, Barsoum M W. X-ray photoelectron spectroscopy of select multi-layered transition metal carbides (MXenes). *Appl Surf Sci* **362**: 406–417 (2016)

[20] Zhou X, Guo Y, Wang D, Xu Q. Nano friction and adhesion properties on Ti_3C_2 and Nb_2C MXene studied by AFM. *Tribol Int* **153**: 106646 (2021)

[21] Zhang D, Ashton M, Ostadhossein A, van Duin A C T, Hennig R G, Sinnott S B. Computational study of low interlayer friction in $Ti_{n+1}C_n$ (n = 1, 2, and 3) MXene. *ACS Appl Mater Interfaces* **9**: 34467–34479 (2017)

[22] Wyatt B C, Rosenkranz A, Anasori B. 2D MXenes: Tunable mechanical and tribological properties. *Adv Mater* **33**: 2007973 (2021)

[23] Tremmel S, Luo X, Rothammer B, Seynstahl A, Wang B, Rosenkranz A, Marian M, Zhu L. Evaluation of DLC, MoS_2, and $Ti_3C_2T_x$ thin films for triboelectric nanogenerators. *Nano Energy* **97**: 107185 (2022)

[24] Zhang X, Xue M, Yang X, Wang Z, Luo G, Huang Z, Sui X, Li C. Preparation and tribological properties of $Ti_3C_2(OH)_2$ nanosheets as additives in base oil. *RSC Adv* **5**: 2762–2767 (2015)

[25] Xue M, Wang Z, Yuan F, Zhang X, Wei W, Tang H, Li C. Preparation of $TiO_2/Ti_3C_2T_x$ hybrid nanocomposites and their tribological properties as base oil lubricant additives. *RSC Adv* **7**: 4312–4319 (2017)

[26] Zhang H, Wang L, Chen Q, Li P, Zhou A, Cao X, Hu Q. Preparation, mechanical and anti-friction performance of MXene/polymer composites. *Mater Des* **92**: 682–689 (2016)

[27] Malaki M, Varma R S. Mechanotribological aspects of MXene-reinforced nanocomposites. *Adv Mater* **32**: 2003154 (2020)

[28] Marian M, Feile K, Rothammer B, Bartz M, Wartzack S, Seynstahl A, Tremmel S, Krauß S, Merle B, Böhm T, et al. $Ti_3C_2T_x$ solid lubricant coatings in rolling bearings with remarkable performance beyond state-of-the-art materials. *Appl Mater Today* **25**: 101202 (2021)

[29] Mai Y J, Li Y G, Li S L, Zhang L Y, Liu C S, Jie X H. Self-lubricating Ti_3C_2 nanosheets/copper composite coatings. *J Alloys Compd* **770**: 1–5 (2019)

[30] Yin X, Jin J, Chen X, Rosenkranz A, Luo J. Ultra-wear-resistant Mxene-based composite coating via in situ formed nanostructured tribofilm. *ACS Appl Mater Interfaces* **11**: 32569–32576 (2019)

[31] Grutzmacher P G, Suarez S, Tolosa A, Gachot C, Song G, Wang B, Presser V, Mücklich F, Anasori B, Rosenkranz A. Superior wear-resistance of $Ti_3C_2T_x$ multilayer coatings. *ACS Nano* **15**: 8216–8224 (2021)

[32] Huang S, Mutyala K C, Sumant A V, Mochalin V N. Achieving superlubricity with 2D transition metal carbides (MXenes) and MXene/graphene coatings. *Mater Today Adv* **9**: 100133 (2021)

[33] Yan H, Zhang L, Li H, Fan X, Zhu M. Towards high-performance additive of Ti_3C_2/graphene hybrid with a novel wrapping structure in epoxy coating. *Carbon* **157**: 217–233 (2020)

[34] Marian M, Tremmel S, Wartzack S, Song G, Wang B, Yu J, Rosenkranz A. Mxene nanosheets as an emerging solid lubricant for machine elements—Towards increased energy efficiency and service life. *Appl Surf Sci* **523**: 146503 (2020)

[35] Marian M, Song G C, Wang B, Fuenzalida V M, Krauß S, Merle B, Tremmel S, Wartzack S, Yu J, Rosenkranz A. Effective usage of 2D MXene nanosheets as solid lubricant—Influence of contact pressure and relative humidity. *Appl Surf Sci* **531**: 147311 (2020)

[36] Nguyen H T, Chung K H. Assessment of tribological properties of Ti_3C_2 as a water-based lubricant additive. *Mater* **13**: 5545 (2020)

[37] Song C, Wang T, Sun X, Hu Y, Fan L, Guo R. Lubrication performance of MXene/Brij30/H2O composite lamellar liquid crystal system. *Colloids Surf A* **641**: 128487 (2022)

[38] Yi S, Li J, Liu Y, Ge X, Zhang J, Luo J. *In-situ* formation of tribofilm with $Ti_3C_2T_x$ MXene nanoflakes triggers macroscale superlubricity. *Tribol Int* **154**: 106695 (2021)

[39] Lian W, Jie X, Lv Y, Yu W. Ti_3C_2/graphene oxide heterostructural coating with enhanced dry tribological performance. *Appl Nanosci* **11**: 1471–1479 (2021)

[40] Miao X, Liu S, Ma L, Yang Y, Zhu J, Li Z, Wang J. Ti_3C_2–graphene oxide nanocomposite films for lubrication and wear resistance. *Tribol Int* **167**: 107361 (2021)

[41] Hirata M, Gotou T, Horiuchi S, Fujiwara M, Ohba M. Thin-film particles of graphite oxide 1: High-yield synthesis and flexibility of the particles. *Carbon* **42**: 2929–2937 (2004)

[42] Song Q, Liu K, Sun W, Chen R, Ji J, Jiao Y, Gao T, Ye J. Lateral and normal capillary force evolution of a reciprocating liquid bridge. *Langmuir* **37**: 11737–11749 (2021)

[43] Song Q, Liu K, Sun W, Ye J. Dead weight microtribometer calibration for improved tolerance to transducer crosstalk and cantilever torsion. *Tribol Lett* **70**: 48 (2022)

[44] Burris D L, Sawyer W G. Addressing practical challenges of low friction coefficient measurements. *Tribol Lett* **35**: 17–23 (2009)

[45] Tanakaa I, Oba F, Sekine T, Ito E, Kubo A, Tatsumi K, Adachi H, Yamamoto T. Hardness of cubic silicon nitride. *J Mater Res* **17**: 731–733 (2002)

[46] Walls M, Chaudhri M, Tang T. STM profilometry of low-load vickers indentations in a silicon single crystal. *J Phys D: Appl Phys* **25**: 500 (2000)

[47] Hamrock B J, Dowson D. Isothermal elastohydrodynamic lubrication of point contacts: part III—fully flooded results. *J Tribol* **99**: 264–275 (1977)

[48] Jacobs T D B, Ryan K E, Keating P L, Grierson D S, Lefever J A, Turner K T, Harrison J A, Carpick R W. The effect of atomic-scale roughness on the adhesion of nanoscale asperities: A combined simulation and experimental investigation. *Tribol Lett* **50**: 81–93 (2013)

[49] Li Y, Huang S, Wei C, Wu C, Mochalin V N. Adhesion of two-dimensional titanium carbides (MXenes) and graphene to silicon. *Nat Commun* **10**: 3014 (2019)

[50] Christenson H. Adhesion and surface energy of mica in air and water. *J Phys Chem* **97**: 12034–12041 (1993)

[51] Chen J, Zhao W. Simple method for preparing nanometer thick Ti_3C_2Tx sheets towards highly efficient lubrication and wear resistance. *Tribol Int* **153**: 106598 (2021)

[52] Rosenkranz A, Gachot C, Erdemir A. Editorial: 2D-layered nanomaterials: Chemical functionalization, advanced characterization, and tribological properties. *Front Chem* **10**: 840213–840213 (2022)

[53] Zhu Y, James D K, Tour J M. New routes to graphene, graphene oxide and their related applications. *Adv Mater* **24**: 4924–4955 (2012)

[54] Li H, Hou Y, Wang F, Lohe M R, Zhuang X, Niu L, Feng X. Flexible all-solid-state supercapacitors with high volumetric capacitances boosted by solution processable MXene and electrochemically exfoliated graphene. *Adv Energy Mater* **7**: 1601847 (2017)

[55] Ghidiu M, Halim J, Kota S, Bish D, Gogotsi Y, Barsoum M W. Ion-exchange and cation solvation reactions in Ti_3C_2 MXene. *Chem Mater* **28**: 3507–3514 (2016)

[56] Du S, Sun J, Wu P. Preparation, characterization and lubrication performances of graphene oxide–TiO_2 nanofluid in rolling strips. *Carbon* **140**: 338–351 (2018)

[57] Sarycheva A, Gogotsi Y. Raman spectroscopy analysis of the structure and surface chemistry of $Ti_3C_2T_x$ MXene. *Chem Mater* **32**: 3480–3488 (2020)

[58] Liu Y, Chen X, Li, J., Luo, J. Enhancement of friction performance enabled by a synergetic effect between graphene oxide and molybdenum disulfide. *Carbon* **154**: 266–276 (2019)

[59] Wu P, Chen X, Zhang C, Luo J. Synergistic tribological behaviors of graphene oxide and nanodiamond as lubricating additives in water. *Tribol Int* **132**: 177–184 (2019)

[60] Dante R C, Kajdas C K. A review and a fundamental theory of silicon nitride tribochemistry. *Wear* **288**: 27–38 (2012)

[61] Grützmacher P G, Rosenkranz A, Rammacher S, Gachot C, Mücklich F. The influence of centrifugal forces on friction and wear in rotational sliding. *Tribol Int* **116**: 256–263 (2017)

[62] Johnson K L, Kendall K, Roberts A D. Surface energy and the contact of elastic solids. *Proc R Soc Edinburgh Sect A: Math Phys Sci* **324**: 301–313 (1971)

[63] Homola A, Israelachvili J, Gee M, McGuiggan P M. Measurements of and relation between the adhesion and friction of two surfaces separated by molecularly thin liquid films. *J Tribol* **111**(4): 675–682 (1989)

[64] Zhang J, Meng Y. Boundary lubrication by adsorption film. *Friction* **3**(2): 115–147 (2015)

[65] Naguib M, Mashtalir O, Lukatskaya M R, Dyatkin B, Zhang C, Presser V, Gogotsiab Y, Barsoum M W. One-step synthesis of nanocrystalline transition metal oxides on thin sheets of disordered graphitic carbon by oxidation of MXenes. *Chem Commun* **50**: 7420–7423 (2014)

[66] Boussaa S A, Kheloufi A, Zaourar N B, Kefaifi A, Kerkar F. Characterization of silica quartz as raw material in photovoltaic applications. *AIP Conf Proc* **1758**: 030043 (2016)

[67] Borovsky B P, Garabedian N T, McAndrews G R, Wieser R J, Burris D L. Integrated QCM-microtribometry: Friction of single-crystal MoS$_2$ and gold from μm/s to m/s. *ACS Appl Mater Interfaces* **11**: 40961–40969 (2019)

[68] Yoon E S, Singh R A, Oh H J, Kong H. The effect of contact area on nano/micro-scale friction. *Wear* **259**: 1424–1431 (2005)

[69] Lipatov A, Lu H, Alhabeb M, Anasori B, Gruverman A, Gogotsi Y, Sinitskii A. Elastic properties of 2D Ti$_3$C$_2$T$_x$ MXene monolayers and bilayers. *Sci Adv* **4**: eaat0491 (2018)

[70] Barrett E P, Joyner L G, Halenda P P. The determination of pore volume and area distributions in porous substances. I. Computations from nitrogen isotherms. *J Am Chem Soc* **73**: 373–380 (1951)

[71] Tang B, Tang C, Chen L, Xiao C, Rosenkranz A, Qian L. Nanoscopic humidity-dependent adhesion behaviors of 2D materials. *Appl Surf Sci* **572**: 151394 (2022)

[72] Persson B N, Scaraggi M. Theory of adhesion: Role of surface roughness. *J Chem Phys* **141**: 124701 (2014)

[73] Marian M, Almqvist A, Rosenkranz A, Fillon M. Numerical micro-texture optimization for lubricated contacts—A critical discussion. *Friction* **10**(11): 1772–1809 (2022)

[74] Milad M, Zreiba N, Elhalouani F, Baradai C. The effect of cold work on structure and properties of AISI 304 stainless steel. *J Mater Process* **203**: 80–85 (2008)

Wei SUN He received his Ph.D. degree in mechanical engineering from Hefei University of Technology in 2022. Dr. Sun's past and current research can be broadly characterized as materials tribology. More specifically his research focuses on minimizing wear and friction of solid lubricant materials with application of polymeric materials and two-dimensional (2D) materials, with a primary focus on understanding and improving the wear of polytetrafluoroethylene (PTFE) composites and blends.

Jiaxin YE. He is a professor in Mechanical Engineering Department at Hefei University of Technology. He majored in mechanical engineering and automation at Tsinghua University in Beijing and received his B.S. degree in 2008. He studied material tribology and solid lubricant design at University of Delaware and received his Ph.D. degree in mechanical engineering in 2014. His research interests are in the area of polymer tribology, liquid friction, and soft material tribology. Current research activities are motivated by challenges in space lubrication, advanced functional surfaces in aerospace, and air pollution control.